Susceptibility of contrail ice crystal numbers to aircraft soot particle emissions

B. Kärcher[1] (ID) and C. Voigt[1,2] (ID)

[1]Deutsches Zentrum für Luft- und Raumfahrt, Institut für Physik der Atmosphäre, Oberpfaffenhofen, Germany, [2]Institut für Physik der Atmosphäre, Johannes Gutenberg Universität, Mainz, Germany

Abstract We develop an idealized, physically based model describing combined effects of ice nucleation and sublimation on ice crystal number during persistent contrail formation. Our study represents the first effort to predict ice numbers at the point where contrails transition into contrail cirrus—several minutes past formation—by connecting them to aircraft soot particle emissions and atmospheric supersaturation with respect to ice. Results averaged over an observed exponential distribution of ice supersaturation (mean value 15%) indicate that large reductions in soot particle numbers are needed to lower contrail ice crystal numbers significantly for soot emission indices around 10^{15} (kg fuel)$^{-1}$, because reductions in nucleated ice number are partially compensated by sublimation losses. Variations in soot particle (−50%) and water vapor (+10%) emission indices at threefold lower soot emissions resulting from biofuel blending cause ice crystal numbers to change by −35% and <5%, respectively. The efficiency of reduction depends on ice supersaturation and the size distribution of nucleated ice crystals in jet exhaust plumes and on atmospheric ice supersaturation, making the latter another key factor in contrail mitigation. We expect our study to have important repercussions for planning airborne measurements targeting contrail formation, designing parameterization schemes for use in large-scale models, reducing uncertainties in predicting contrail cirrus, and mitigating the climate impact of aviation.

Plain Language Summary The formation and modification of ice crystals in persistent aircraft condensation trails (contrails) is an important component in evaluating the climate impact of aviation. We connect for the first time contrail ice numbers at the end of the formation stage to aircraft soot emissions and atmospheric ice supersaturation. We offer a framework to estimate changes in ice number and to compare effects of mitigation options. Our results show that large reductions in soot emissions are required to lower contrail ice numbers significantly, and those ice numbers are insensitive to small variations of the amount of water vapor emitted by aircraft jet engines. Our study has important implications for planning field measurements, reducing uncertainties in numerical predictions of contrail cirrus effects on climate and for mitigating this impact.

1. Introduction

Contrail cirrus clouds evolving from line-shaped contrails significantly perturb the planetary radiation balance [*Boucher et al.*, 2013]. The formation and modification of ice crystals in persistent contrails is one important component in evaluating the climate impact of contrail cirrus evolving from them. Air travel volume and therefore contrail-induced cloudiness is expected to increase in the future. In seeking ways to parameterize contrail ice formation, physical processes affecting ice crystals in the contrail formation stage must be well understood and quantified.

In the contrail formation stage (Figure 1), ice crystals nucleate and grow by water vapor deposition in jet engine exhaust plumes and sublimate subsequently in aircraft wakes. These processes pave the way for the further development of mean ice crystal size, contrail cirrus coverage, and other cloud properties in the spreading stage. Previous studies explained how nucleated ice crystal concentrations change with jet engine soot particle emissions and other aircraft-related factors [*Wong and Miake-Lye*, 2010; *Kärcher et al.*, 2015] and also suggested that a fraction of ice crystals are lost by subsequent sublimation in aircraft wake vortices [*Lewellen*, 2012; *Unterstrasser*, 2016]. This fraction depends nonlinearly on nucleated ice crystal numbers, hence, engine soot emissions, and ambient relative humidity. It is therefore important to estimate the combined effect of nucleation and sublimation on contrail ice crystal numbers.
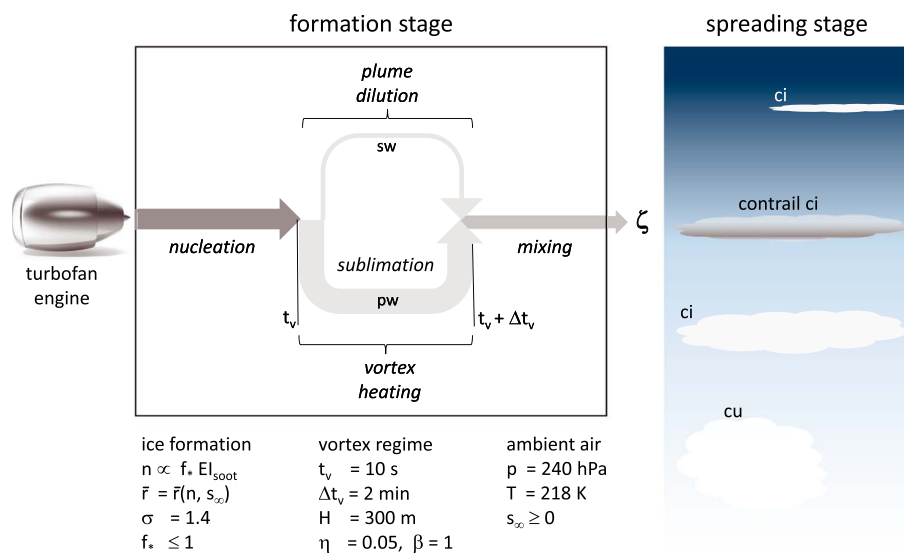
Figure 1. Key processes and model parameters (baseline values) determining the ice formation efficiency, ζ, in persistent contrails. The aircraft-dominated formation stage covers jet, vortex, and dissipation regimes and lasts about 5–10 min [*Paoli and Shariff*, 2016]. Jet exhaust plumes emanate from individual aircraft engines in which contrail ice crystals form within the first second past emission mainly from engine soot emissions. The plumes entrain ice supersaturated ambient air ($s_\infty \geq 0$) and therefore allow ice crystals to grow by uptake of the supersaturated water vapor. While the total number concentration of ice crystals, n, dilutes, their mean radius, $\bar{r}$, tends to increase after formation. At the same time, the jet plumes roll up into a pair of trailing vortices generated near the wing tips. At plume ages $t_v \simeq 5$–20 s, the sinking vortices, in which entrainment is strongly suppressed, stabilize below the flight level forming the primary wake (pw). A small fraction of exhaust is detrained from the jet plumes during roll up forming a secondary wake (sw), in which n dilutes further around flight level at temperature, T, and pressure, p; $\bar{r}$ increases due to continual in mixing and deposition of ambient water vapor. The vertical displacement of pw, $H \simeq 150$–400 m, is determined by the vortex circulation (proportional to aircraft weight) and the ambient stratification (embodied in the Brunt-Väisälä frequency) and is therefore larger for heavier aircraft and in calmer (less turbulent) atmospheric conditions. The sinking lasts $\Delta t_v \simeq 2$–3 min, depending on aircraft properties and ambient conditions; it leads to a warming of the air captured in it, hence, potentially to complete sublimation of ice crystals. Eventually, the organized wake vortex flow field collapses and mixes (dissipates) around $t_v + \Delta t_v$. The parameter η is used to estimate wake-averaged contrail ice crystal numbers, hence, the fraction of nucleated ice crystals that remain in the atmospheric spreading stage, in which contrails transition into contrail cirrus.

To date, observational and modeling studies combining the full suite of processes that would allow us to predict with confidence initial ice crystal numbers in contrail cirrus are lacking. Parcel models treat ice nucleation and growth in detail but do not cover the sublimation phase and simplify transport and mixing. Large eddy simulations (LES) combine fluid dynamics with ice growth and sublimation but do not treat the crucial nucleation phase. This hampers proper initialization of contrail cirrus parameterizations in climate models. Mitigation strategies aiming at reducing those effects are difficult to develop.

The goals of this study are twofold: first, to quantify contrail ice numbers by combining effects of all key microphysical processes involved in contrail formation together (section 2), including a comparison to aircraft observations and numerical simulations (section 3) and second, to propose a methodology—introducing the ice formation efficiency and its susceptibility to soot emissions as central variables—useful for assessing options to reduce the contrail cirrus climate impact by targeting the contrail formation stage (section 4).

2. Wake Processing of Ice Crystals in Persistent Contrails

2.1. Conceptual Model

The underlying conceptual framework-sketched Figure 1 is borne out by airborne observations [*Voigt et al.*, 2010] and LES [*Paoli and Shariff*, 2016]. The ice crystal sublimation efficiency, ξ, defines the ratio between contrail ice crystal number concentrations (per unit volume of air) before (plume age t_v) and after ($t_v + \Delta t_v$) wake vortex processing

$$\xi = \frac{n(t_v + \Delta t_v)}{n(t_v)} = \underbrace{(1-\eta)f_{\text{pw}}}_{\text{primary wake (pw)}} + \underbrace{\eta \mathcal{D}_{\text{sw}}}_{\text{secondary wake (sw)}} . \tag{1}$$

While $n(t_v)$ decreases by isobaric mixing by a factor $\mathcal{D}_{sw}$ in the fraction of detrained exhaust, it is affected by sublimation losses in the exhaust trapped in the sinking (heating) vortices in which mixing is strongly suppressed. The ice crystal fraction remaining in pw after sublimation is given by f_{pw}, whereby a small adiabatic change in n is neglected. During wake dissipation, ice crystals that experienced different dynamical and microphysical histories in pw and sw mix. A fractional weighting factor η is used to define the total ice crystal number concentration as an average over the two contributions; η is related to part of the exhaust detrained from the jet plumes at t_v, which typically constitutes a small fraction of the total exhaust.

Wake mixing, entrainment, and detrainment processes are complex [*Sussmann*, 1999; *Guignery et al.*, 2012]. Encapsulating their net effect on n into a single parameter, η, is a simplification that allows us to formulate an approximate description of factors controlling contrail ice crystals across the whole formation stage. Contrail structure is affected by atmospheric and self-induced aircraft turbulence. In particular, pw and sw are not entirely disconnected as suggested in Figure 1, affecting both f_{pw} and η. In this study, we develop a model predicting f_{pw} without addressing wake interactions and view η as a fit parameter that is not predicted by the model.

The air in pw warms adiabatically at a rate $\omega_{heat} = \theta\,\dot{T}/T^2$, where $\theta(T)$ is the latent heat of sublimation expressed in temperature units. This rate follows from the Clausius-Clapeyron relationship neglecting a small change in the partial pressure of water vapor. The vortex heating rate is estimated from $\dot{T} \simeq H\Gamma/\Delta t_v$, where Γ is the absolute value of the lapse rate. Baseline values for ambient contrail conditions and for H, t_v, Δt_v, and η, suitable for large aircraft at cruise, are given in Figure 1. This yields $\mathcal{D}_{sw} \simeq [t_v/(t_v + \Delta t_v)]^\beta = 1/13$ ($\beta = 1$), $\dot{T} \simeq 1\,\text{K min}^{-1}$ and $\omega_{heat} \approx 0.1\,\text{min}^{-1}$. The supporting information provides this relationship along with typical values of parameters, such as the water vapor diffusion coefficient, D, and the length scale, a, separating ice crystal deposition growth regimes based on *Lamb and Verlinde* [2011], as well as the relationship between soot particle emission indices, EI_{soot}, and nucleated contrail ice crystal number concentrations, $n_\star$, based on our ice formation parameterization [*Kärcher et al.*, 2015]. At the point where most ice crystals form (subscript $\star$), i.e., at a plume age around $t_\star = 0.3$ s, we fix the fraction of soot emissions that form ice, $f_\star = 1$, ice supersaturation, $s_\star = 0.5$, mean ice crystal radius, $\bar{r}_\star = 0.3\,\mu\text{m}$, and plume temperature, $T_\star = 231$ K. These values—typical for many contrails in cruise conditions—are allowed to vary with soot particle emissions and ambient ice supersaturation in section 4.

To predict depositional growth and sublimation of contrail ice crystals at the same level of approximation as in our ice formation model, we introduce a general equation for the temporal evolution of bulk plume or wake ice supersaturation, s

$$\frac{ds}{dt} = -\ \underbrace{\omega_{mix}(s - s_\infty)}_{\text{entrainment mixing}} - \underbrace{\omega_{micro}s}_{\text{quenching}} - \underbrace{\omega_{heat}(s + 1)}_{\text{heating}}\,. \tag{2}$$

Initial conditions for s and process rates, ω_{mix} and ω_{micro}, are specified in sections 2.2 and 2.3. In the absence of mixing ($\omega_{mix} = 0$), equation (2) expresses conservation of total water during ice crystal growth ($s > 0$) or sublimation ($s < 0$).

2.2. Ice Crystal Growth in the Late Jet Regime

We derive relationships for n and $\bar{r}$ at $t = t_v$ in the late jet regime right before sublimation is assumed to occur. The nucleated ice crystal number concentration declines by dilution in individual jet plumes between the time of formation, $t_\star$, and t_v according to

$$n_v \equiv n(t_v) = n_\star \left(\frac{t_\star}{t_v}\right)^\beta\,, \quad n_\star\,[\text{cm}^{-3}] \simeq 2 \times 10^{-10}\,f_\star\,\text{EI}_{soot}\,[(\text{kg–fuel})^{-1}]\,. \tag{3}$$

Ice crystals grow or sublimate according to

$$\frac{dr}{dt} = \frac{Gs}{r + a}\,, \quad G = \nu D(p, T)n_{sat}(T)\,; \tag{4}$$

the growth factor G per unit supersaturation is proportional to the number density of water molecules at ice saturation, n_{sat}, and the volume of a water molecule in ice, ν. Equation (4) describes the rate of change of the volume mean radius r governed by an effective diffusion coefficient, $D/(1 + a/r)$. For small or sublimating ice crystals in young contrails, $r \leq a$, therefore, it is important to include this correction to D.

While supersaturated ambient water vapor is mixed into the young jet plume at $t = t_\star$ at a rate $\omega_{mix} = 1/t_\star$, the plume supersaturation is depleted at the rate $\omega_{micro} = 4\pi \bar{r}_\star^2 n_\star D/(\bar{r}_\star + a)$. For high $n_\star$, corresponding to $EI_{soot} > 10^{14}$ (kg fuel)$^{-1}$, s diminishes rapidly limiting ice crystal growth, consistent with in situ measurements [*Kaufmann et al.*, 2014]. This happens because the ice crystals deplete the vapor at a faster rate than it is resupplied by mixing ($\omega_{micro} > \omega_{mix}$). By contrast, for lower EI_{soot}, s comes closer to its value in ambient air, s_∞, leading to slower uptake for $\omega_{micro} < \omega_{mix}$. In such cases, for high s_∞ values, ice crystals can grow to sizes much larger than $\bar{r}_\star$ by t_v since they benefit from the high levels of ambient moisture.

When applied to $\bar{r}$, equation (4) is solved assuming constant G and a

$$\bar{r}_v \equiv \bar{r}(t_v) = \sqrt{(\bar{r}_\star + a)^2 + 2G \int_{t_\star}^{t_v} s(t)\,dt} - a\,, \tag{5}$$

where the integral is a measure of the water vapor mass deposited on the ice crystals within $(t_v - t_\star)$, obtained from the solution of equation (2) with $\omega_{heat} = 0$. In this case, the resulting equation models the quenching (relaxing toward saturation) of supersaturation at constant ω_{micro} and the generation of s by entrainment mixing at variable $\omega_{mix} = 1/t$. It has the solution

$$s(\tau) = \frac{s_\infty}{\lambda \tau} + \left(s_\star - \frac{s_\infty}{\lambda}\right) \frac{e^{-\lambda(\tau-1)}}{\tau}\,, \quad \lambda = \frac{\omega_{micro}}{\omega_{mix}}\,, \tag{6}$$

with the scaled plume age $\tau = t/t_\star$ and the dimensionless jet regime parameter λ taken at $t = t_\star$. The initial ice supersaturation, $s_\star$, is generated by high-engine water vapor emissions and rapid plume cooling. Integrating equation (6) between $t = t_\star$ ($\tau = 1$) and $t = t_v$ ($\tau = \tau_v$) yields

$$\int_{t_\star}^{t_v} s(t)\,dt = \left\{ \left(s_\star - \frac{s_\infty}{\lambda}\right) \int_1^{\tau_v} \frac{e^{-\lambda(\tau'-1)}}{\tau'}\,d\tau' + \frac{s_\infty}{\lambda} \ln \tau_v \right\} t_\star \tag{7}$$

used to estimate $\bar{r}_v$ from equation (5).

2.3. Ice Crystal Sublimation in the Vortex Regime

We estimate values $s = s_v$ driving sublimation in the primary wake. We consider adiabatic heating as a loss rate for the supersaturation tendency and sublimation as a production rate by applying equation (2) with $\omega_{mix} = 0$. With constant process rates, ω_{heat} from section 2.1 and $\omega_{micro} = 4\pi \bar{r}_v^2 n_v D/(\bar{r}_v + a)$ evaluated with n_v from equation (3) and $\bar{r}_v$ from equation (5), the quasi-steady state solution ($ds/dt = 0$) reads

$$s_{qss} = -\frac{1}{1 + \mu}\,, \quad \mu = \frac{\omega_{micro}}{\omega_{heat}}\,, \quad \tau_s = \frac{1}{\omega_{micro} + \omega_{heat}}\,, \tag{8}$$

introducing the dimensionless vortex regime parameter μ taken at $t = t_v$. The steady state is approached exponentially on the supersaturation quenching time scale τ_s

$$s(t \geq t_v) = s_{qss} + (\bar{s} - s_{qss}) \exp[-(t - t_v)/\tau_s]\,, \tag{9}$$

where $\bar{s} = s(t_v)$ denotes the value of s in evolving jet plumes at plume age t_v from equation (6) that serves as an initial condition for equation (9). In turn, equation (9) taken at $t = t_v + \Delta t_v$ leads to

$$\hat{s}_v = s_{qss} + (\bar{s} - s_{qss}) \exp(-\Delta t_v/\tau_s)\,. \tag{10}$$

While $\hat{s}_v$ denotes the ambient value of s, the actual value over the surface of individual ice crystals, s_v, should be corrected for the size-dependent curvature (Kelvin) effect

$$s_v = \hat{s}_v - s_K\,; \quad s_K = \exp\left(\frac{a_K}{\bar{r}_v}\right) - 1 \simeq \frac{a_K}{\bar{r}_v}\,, \tag{11}$$

with the Kelvin radius $a_K(T) \ll \bar{r}_v$. For typical contrail temperatures, we use a constant baseline value, $a_K = 2$ nm. The curvature correction for individual ice crystals is highly uncertain, first, because of the poorly constrained Kelvin radius, a_K, and second, because we apply this correction to a population of particles with different sizes outside equation (4). This creates uncertainty in the pw contribution to ξ (equation (1)) for high ice crystal numbers. *Lewellen* [2012] and subsequent LES studies [e.g., *Naiman et al.*, 2011] pointed out the importance of the Kelvin effect in contrails. This seems surprising, since $s_K = \mathcal{O}(10^{-3})$ is very small. While this effect is indeed negligible in natural cirrus clouds, it is important in the contrail vortex regime due to high ice crystal number concentrations, especially in ambient air near ice saturation ($s_\infty \approx 0$). We explain this by rapid

sublimation time scales: for $n_v = 6000$ cm^{-3} (corresponding to EI$_{soot}$ = 10^{15} (kg fuel)$^{-1}$) and $\bar{r}_v \simeq 1$ μm, we find $1/\omega_{micro} \simeq 1/3$ s indicating the strong tendency of sublimation to restore ice saturation in pw.

The supersaturation quenching time scale τ_s is shorter than t_v the higher n_v. In such cases, $\tau_s \to 1/\omega_{micro}$ and sublimation restores ice saturation in jet plumes very effectively almost regardless of s_∞, so that $\hat{s}_v \to 0$ and $s_v \simeq -s_K$. For EI$_{soot}$ = 10^{15} (kg fuel)$^{-1}$ and $s_v = -s_K = -0.001$, the sublimation tendency $\omega_{micro}|s_v| \simeq 0.2$ min^{-1} is comparable to the heating tendency $\omega_{heat}(s_v + 1) \simeq \omega_{heat} \simeq 0.1$ min^{-1}.

Hence, for high ice crystal concentrations, sublimation losses are dominated by the Kelvin effect and are largely independent of ambient supersaturation, in line with LES predictions [*Unterstrasser*, 2016]. By contrast, for sufficiently low total ice crystal numbers, the water vapor-ice interaction is kinetically hindered and $\tau_s \to 1/\omega_{heat} \simeq 10$ min is determined by the heating rate imposed on the wake vortices. In those cases, since $\tau_s > t_v$, s_v assumes large negative values, lessening the importance of the Kelvin effect. The values of n_v satisfying $\tau_s > t_v$ are $n_v < 100$ cm^{-3}, roughly corresponding to EI$_{soot}$ < 10^{13} (kg fuel)$^{-1}$. At those low ice numbers outside soot-rich conditions, the assumption of constant s_v driving sublimation at constant p and T over the whole pw sinking time, Δt_v, likely becomes unrealistic. Microphysical processes are no longer slaved to fluid dynamical changes.

We modify the solution behavior at low n_v values by reducing Δt_v in equation (10) to $\delta t_v = \Delta t_v \exp[-\gamma \max\{0, (\tau_s - t_v)\}/\Delta t_v]$ with the empirical parameter $\gamma \geq 0$; this shortens the time during which s_v is used to estimate sublimation losses in cases where our model possibly ceases to be applicable (i.e., $\tau_s > t_v$ for sufficiently low n_v). The model modified with $\gamma = 3$ works for EI$_{soot}$ > 2×10^{13} (kg fuel)$^{-1}$ in contrails well below thermodynamic formation thresholds (typically around 255 K), as judged by a comparison to LES results (section 3).

The fraction of ice crystals trapped in pw escaping complete sublimation, f_{pw}, is estimated based on a normalized ice crystal size distribution (PSD), $F(r, t) = (1/n_v) \, dn/dr$. The equation governing F reads

$$\frac{\partial F}{\partial t} + \frac{\partial}{\partial r}\left(\frac{dr}{dt}F\right) = 0 \tag{12}$$

and is solved with equation (4) for constant G, a, and s to estimate f_{pw} (see supporting information). Shape and width of ice crystal PSDs in young contrails are virtually unconstrained. A lognormal PSD is used for initialization, with $\bar{r} = \bar{r}_v \exp(-1.5 \ln^2 \sigma_v)$ and σ_v indicating the mode radius and geometric standard deviation at t_v, respectively. Values $\sigma_v > 1$ are used to account for spectral broadening due to turbulent mixing of air parcels with different supersaturation histories. The solution of equation (12) is a Gaussian distribution in the auxiliary variable $z(r, t)$ defined over the range $[z_{min}, \infty]$:

$$z_{min}(t) = z(r = 0, t = t_v + \delta t_v) = \frac{\ln\left\{\left(\sqrt{a^2 - 2Gs_v\delta t_v} - a\right)/\bar{r}\right\}}{\sqrt{2}\ln\sigma_v} = \frac{\ln \mathcal{Z}}{\sqrt{2}\ln\sigma_v} \geq -\infty. \tag{13}$$

Complete sublimation is assumed to occur at $r = 0$ because contrail ice crystal core particles are very small (10–100 nm); then f_{pw} follows from

$$f_{pw} = \int_0^\infty F(r, t = t_v + \delta t_v) \, dr = \frac{1}{2}[1 - \text{erf}(z_{min})] \simeq \frac{1}{1 + \mathcal{Z}^k}; \quad k = \frac{4}{\sqrt{2\pi}\ln\sigma_v}, \tag{14}$$

where $\text{erf}(y) = (2/\sqrt{\pi})\int_0^y e^{-x^2} \, dx$ is the error function.

3. Comparison With In Situ Observations and LES Results

Figure 2a compares sublimation efficiencies as a function of soot particle number per kilogram of fuel burnt (emission index) with LES results computed for a large aircraft at cruise at different ambient ice supersaturation. To compare directly with the LES, we use the number emission index-based version of equation (1), reading

$$\xi_{EI} = (1 - \eta)f_{pw} + \eta; \tag{15}$$

emission indices in sw are not affected by dilution; hence, $\mathcal{D}_{sw} = 1$. Given that case-by-case variability in the LES data points has not been accounted for in this comparison, we judge the agreement favorable. Importantly, our model predicts similar trends $\xi_{EI}(\text{EI}_{soot})$ and $\xi_{EI}(s_\infty)$ increasing confidence that it captures the most relevant physical processes affecting sublimation.
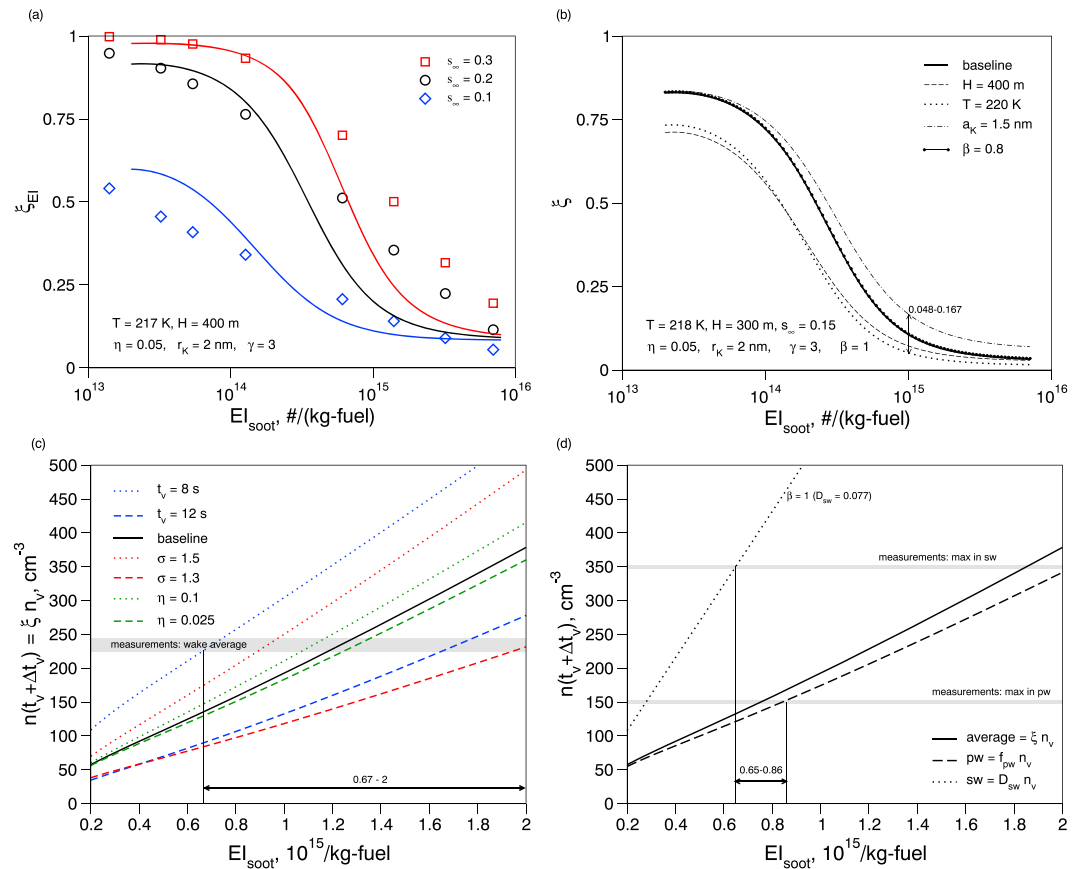
Figure 2. (a) Overall number emission index-based sublimation efficiency, ξ_{EI}, from this work for $T = 217$ K and $H = 400$ m (solid curves) and from LES (open symbols) [*Unterstrasser*, 2016, Table 2, Block 4] computed for the same EI_{soot} and s_∞ values but for T and H values that differ on a case-by-case basis. (b) Overall number concentration-based sublimation efficiency, ξ, for baseline parameters and $s_\infty = 0.15$ [*Gierens et al.*, 1999], including curves obtained by variation of selected parameters. The double arrow indicates the estimated range of uncertainty for ξ in this model for soot-rich contrails. (c) Comparison of modeled, wake-averaged total ice crystal number concentrations after vortex processing (curves) with in situ measurements (gray bar) behind an Airbus A380 aircraft at $p = 242$ hPa, $T = 218$ K, and $s_\infty = 0$ (CONCERT campaign) [*Jeßberger et al.*, 2013] versus EI_{soot} including variations of model parameters. The range of assumed EI_{soot} values consistent with measured concentrations (double arrow) is higher than the value $\approx 2.5 \times 10^{14}$ (kg fuel)$^{-1}$ estimated based on engine calculations, supporting an earlier analysis [*Schumann et al.*, 2013]. (d) Comparison of the same observational data set reporting maximum ice crystal concentrations separately in pw and sw (gray bars) [*Gayet et al.*, 2012] with this model using baseline parameters. The double arrow indicates the possible range of EI_{soot} values satisfying those data. In all cases, EI_{soot} values equal nucleated apparent ice crystal emission indices if $f_\star = 1$.

Figure 2b shows number concentration-based sublimation efficiencies, ξ, assuming a mean value for ice supersaturation ($s_\infty = 0.15$) in upper tropospheric air taken along actual aircraft flight routes. Variations of physical variables (H, T) and model parameters (a_K, β) result in a notable spread of ξ values amounting to a factor 3.5 at $EI_{soot} = 10^{15}$ (kg fuel)$^{-1}$. This factor is caused by mild variations in T and a_K alone; varying the dilution factor, $\mathcal{D}_{sw}$, from 0.077 ($\beta = 1$) to 0.1 ($\beta = 0.8$) has little effect on ξ, because the sw contribution to ξ has been assigned only a small weight ($\eta = 0.05$).

Aircraft measurements were taken in the inhomogeneous primary and secondary wakes of a contrailing, heavy aircraft at plume ages $102-115$ s, quantifying number concentrations of contrail particle with diameters exceeding ≈ 1 μm, interpreted as ice crystals. The soot particle emission index was not measured; dilution histories have not been reported, and ambient relative humidity close to ice saturation was uncertain (we use $s_\infty = 0$ in the analysis).

The model results shown in Figure 2c are sensitive to small variations in t_v. This highlights the potential importance of capturing the jet plume conditions $\{\bar{r}_v, s_v, \sigma_v\}$ just prior to vortex processing when estimating

the sublimation losses. The sensitivity studies indicate that EI_{soot} might have been in the range $(0.67-2){\times}10^{15}$ (kg fuel)$^{-1}$. This might suggest that contrail far-field measurements of wake-averaged ice crystal number concentrations do not allow to constrain EI_{soot} values well, probably no better than within a factor of 3, when taking into account all parameter sensitivities in this idealized model. This underscores the importance of measuring AEI simultaneously with EI_{soot} to better relate ice numbers to soot emissions. We infer a tighter constraint by comparing individual pw and sw ice crystal number concentrations in Figure 2d: $EI_{soot} \approx (0.65-0.86){\times}10^{15}$ (kg fuel)$^{-1}$. However, predicted pw, sw, and wake-averaged ice crystal concentrations do not simultaneously agree with the data using a single EI_{soot} value. This uncertainty arises because the full wake depth was not probed and transport of some air parcels processed in pw back into sw at the time of the measurements cannot be ruled out.

4. Implications for Mitigation

The apparent emission index of contrail ice crystals at the end of the formation stage is written for soot-rich contrails ($EI_{soot}>10^{13}$ (kg fuel)$^{-1}$) as

$$AEI = \zeta \cdot EI_{soot}, \qquad \underbrace{\zeta}_{\text{formation efficiency}} = \underbrace{f_\star}_{\text{nucleation efficiency}} \cdot \underbrace{\xi_{EI}}_{\text{sublimation efficiency}}, \qquad (16)$$

where both, $f_\star$—computed in this section from the contrail ice formation model [*Kärcher et al.*, 2015] along with $\{r_\star, s_\star, t_\star\}$ for given $\{EI_{soot}, s_\infty\}$ and aircraft-related parameters—and ξ_{EI} [*Unterstrasser*, 2016] (and symbols in Figure 2a) depend nonlinearly on EI_{soot}. The term "apparent" indicates that contrail ice crystals do not belong to engine emissions. The ice formation efficiency, ζ, is a characteristic of the contrail formation stage and incorporates the impact of ice crystal nucleation and sublimation on AEI. The susceptibility, κ, of ice crystal number to soot emissions is related to ζ via

$$\kappa \equiv \frac{\partial \ln AEI}{\partial \ln EI_{soot}} = 1 + \frac{\partial \ln \zeta}{\partial \ln EI_{soot}} = 1 + \frac{\partial \ln f_\star}{\partial \ln EI_{soot}} + \frac{\partial \ln \xi_{EI}}{\partial \ln EI_{soot}}, \qquad (17)$$

split into its jet and vortex regime contributions; both are not independent. Changes in emissions (e.g., soot particles or water vapor) or aircraft and engine/fuel properties (e.g., overall propulsive efficiency or fuel energy content) affect the former contribution, while the latter depends markedly on ambient ice supersaturation and accounts for the sublimation-related response to those changes. To aid systematic studies of s_∞ effects in persistent contrails, it may be useful to define a related susceptibility, $\partial \ln AEI / \partial \ln s_\infty$. Equations (16) and (17) must be redefined in the case of soot-poor contrails to include effects of ambient aerosols.

Figure 3 shows the EI_{soot} dependence of ζ, κ, and AEI, averaged over an observation-based, exponential probability distribution of ambient ice supersaturation. The agreement of our model results for AEI with the measurements discussed in Figure 2 is encouraging. In soot-rich contrails forming well below the thermodynamic threshold temperatures, $f_\star \simeq 1$, hence, $\zeta \simeq \xi_{EI}$. Ice crystal sublimation in the vortex regime causes the susceptibility, κ, to drop below unity—the value characteristic for the late jet regime [*Kärcher*, 2016, Figure 3a] —and to attain a minimum around $EI_{soot}=10^{15}$ (kg fuel)$^{-1}$. The minimum in κ develops since reductions in AEI due to reductions in EI_{soot} are most strongly compensated by decreased sublimation losses (increasing ζ). At the lowest soot levels discussed here, κ increases since ζ starts to level off. We therefore expect that in soot-poor conditions, where initial ice numbers are controlled by ambient aerosol particles, the already low levels of AEI can further be reduced by avoiding atmospheric regions with high-aerosol particle number concentrations.

Generally, the overall effect on AEI by reducing EI_{soot} depends notably on s_∞ [*Unterstrasser*, 2014, 2016]. The decrease in AEI due to the use of biofuel blends at average ambient ice supersaturation is limited (open circles in Figure 3b) and decreases with diminishing s_∞. Some biofuel blends emit slightly higher levels of water vapor than conventional fuel [*Moore et al.*, 2015, 2017]. This increases peak liquid water supersaturation in aircraft exhaust plumes [*Kärcher*, 2016] and tends to simultaneously increase ice crystal number and sublimation losses due to opposing changes in ζ, resulting in a small combined effect on AEI (dash-dotted curve). This also implies that the effectiveness of technological contrail avoidance strategies aiming at reducing ice crystal formation by lowering the levels of plume supersaturation [*Noppel and Singh*, 2007] is reduced, since lower AEI at formation due to lower plume supersaturation [*Kärcher*, 2016] provokes reduced sublimation losses, likewise dampening the net change of AEI at the end of the formation stage.
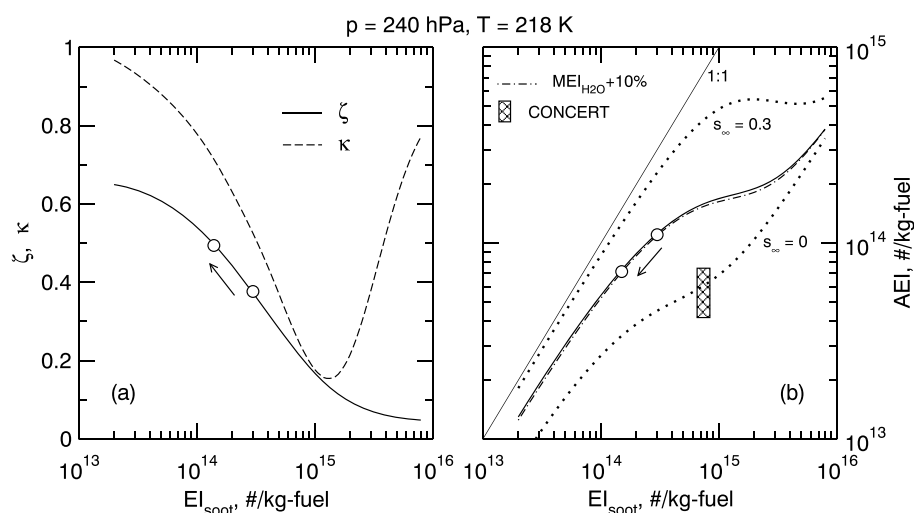
Figure 3. (a) Contrail ice formation (combined nucleation and sublimation) efficiency, ζ, ice number susceptibility, κ, and (b) apparent ice crystal number emission index, AEI, at the end of the contrail formation stage versus aircraft soot particle number emission index, EI_{soot}. The 1:1 line in Figure 3b indicates peak AEI values for maximum ice formation efficiency ($\zeta = 1$). All quantities were evaluated using baseline parameter values for a heavy aircraft and weighted with an exponential probability distribution function of ambient ice supersaturation (mean value: 0.15) guided by in situ measurements along actual aircraft flight routes [*Gierens et al.*, 1999], except the dotted curves in Figure 3b that were obtained at single s_∞ values marking lower and (approximate) upper limit bounds on AEI. Circles and arrows indicate that a 50% reduction in EI_{soot} at maximum range thrust, from 3×10^{14} (kg fuel)$^{-1}$ to 1.5×10^{14} (kg fuel)$^{-1}$ due to the use of biofuel blending as observed during ACCESS [*Moore et al.*, 2017], increases ζ by 31% and decreases average AEI by 35%. Relative changes in AEI are smaller at higher EI_{soot} values, especially near the region of minimum susceptibility around $EI_{soot} = 10^{15}$ (kg fuel)$^{-1}$. A sensitivity study in which the water vapor mass emission index, MEI_{H_2O}, has been increased by 10% above the nominal value 1.25 g (kg fuel)$^{-1}$ shows only a very small effect on AEI (dash-dotted curve). The filled square indicates the range of results for the ice-saturated ($s_\infty = 0$) observation case (CONCERT) analyzed in Figure 2.

5. Conclusions

Dynamical and microphysical elements of ice crystal evolution in the aircraft wake vortex regime must be known well to constrain ice crystal numbers at the end of the contrail formation stage. Ice crystal sublimation in sinking wake vortices depends nonlinearly on soot emissions and atmospheric supersaturation. While wake vortex processing in soot-rich contrails counteracts the effect of initial reductions in ice crystal number through sublimation losses, reductions in soot particle numbers at emission always lead to lower ice crystal number concentrations in spreading contrail cirrus. The main purpose of our approximate model is to enhance understanding of how different processes work together to affect contrail ice numbers right before persistent contrails transition into contrail cirrus. Its quantitative predictions may further be validated with the help of observations and numerical simulations over a range of soot emissions and ambient ice supersaturation levels. In this regard, we suggest that future LES models include appropriate parameterizations of contrail water droplet and ice formation from plume particle precursors. This would enable a consistent evaluation of the ice formation efficiency and susceptibility to soot emissions across the whole contrail formation stage. Uncertainties in AEI should be systematically explored, for instance, those caused by the Kelvin effect in soot-rich contrails and those caused by kinetic limitations to ice crystal growth in contrails with low ice crystal number concentrations (in soot-poor or near-threshold contrails). Aircraft observations might specifically target the sublimation loss mechanism in primary wake vortices in persistent contrails.

For current (soot-rich) emissions, reducing EI_{soot} is an efficient means to reduce contrail ice numbers. This reinforces the notion that the formation stage bears a large potential for mitigation. However, large variations in soot particle and water vapor emission indices (exceeding those caused by the use of biofuel blends) are required to affect ice crystal numbers strongly. Once soot-poor conditions are achieved, avoiding atmospheric regions of high-aerosol particle number concentrations during contrail formation reduces ice crystal numbers further. We suggest to explore in greater detail aerosol and fluid dynamical influences on contrail ice crystal numbers at the end of the formation stage using observationally based and process model-constrained

estimates of the ice formation efficiency and susceptibility as a function of soot emissions and ambient ice supersaturation. Moreover, we suggest to account for variable contrail ice numbers in climate models, based on emission inventories providing variability in soot emissions and on subgrid parameterizations of relative humidity in the models' cloud schemes [*Burkhardt et al.*, 2008] providing supersaturation variability.

With regard to mitigation, the methodology proposed here facilitates the comparison of options aiming at reducing the contrail cirrus climate impact. It allows the system-wide behavior of the contrail formation process to be studied by detailed analyses of distinct but coupled subcomponents, the ice nucleation efficiency pertinent to the jet regime, and the sublimation efficiency pertinent to the vortex regime of aircraft wake development.

Acronyms

pw	primary wake
sw	secondary wake
ACCESS	Alternative Fuel Effects on Contrails and Cruise Emissions
CONCERT	Contrail and Cirrus Experiment
LES	large-eddy simulation
PSD	contrail ice crystal size distribution

Notation

$\star$	subscript indicating conditions at ice nucleation
∞	subscript indicating conditions in ambient air
ad	subscript indicating adiabatic change
micro	subscript indicating microphysics
mix	subscript indicating jet plume mixing
soot	subscript indicating soot particle emission
s	subscript indicating supersaturation
v	subscript indicating beginning of vortex regime
K	subscript associated with Kelvin effect
a	characteristic radius
f	ice nucleation efficiency; fraction after sublimation
n	total ice crystal number density
p	air pressure
r ($\bar{r}$)	ice crystal radius (volume mean radius)
s	supersaturation with respect to ice
t (Δt, δt)	plume age (duration of sublimation)
x, z, Z	auxiliary variables
D	plume dilution factor
AEI	apparent ice crystal number emission index
EI (MEI_{H_2O})	particle number (water vapor mass) emission index
F	normalized ice crystal size distribution
G	ice crystal growth/sublimation rate factor
H	maximum contrail depth
T ($\dot{T}$)	air temperature (vortex heating rate)
β	parameter in plume dilution factor
η	factor for averaging ice crystal numbers across the wake
κ	susceptibility of ice number to soot emissions
λ, μ	ratio of process rates
σ	geometric standard deviation of lognormal PSD
ω	process rate
τ	characteristic time scale
ζ	ice formation efficiency
ξ (ξ_{EI})	sublimation efficiency (EI-based)
Γ	dry lapse rate

References

Burkhardt, U., B. Kärcher, M. Ponater, K. Gierens, and A. Gettelman (2008), Contrail cirrus supporting areas in model and observations, *Geophys. Res. Lett.*, *35*, L16808, doi:10.1029/2008GL034056.

Boucher, O., et al. (2013), Clouds and aerosols, in *Climate Change 2013: The Physical Science Basis. Contribution of Working Group I to the Fifth Assessment Report of the Intergovernmental Panel on Climate Change*, edited by T. F. Stocker et al., pp. 571–658, Cambridge Univ. Press, Cambridge, U. K., and New York, doi:10.1017/CBO9781107415324.016.

Gayet, J.-F., et al. (2012), The evolution of microphysical and optical properties of an A380 contrail in the vortex phase, *Atmos. Chem. Phys.*, *12*, 6629–6643.

Gierens, K., U. Schumann, M. Helten, H. G. J. Smit, and A. Marenco (1999), A distribution law for relative humidity in the upper troposphere and lower stratosphere derived from three years of MOZAIC measurements, *Ann. Geophys.*, *17*, 1218–1226.

Guignery, F., E. Montreuil, O. Thual, and X. Vancassel (2012), Contrail microphysics in the near wake of a realistic wing through RANS simulations, *Aerosol Sci. Technol.*, *23*, 399–408.

Jeßberger, P., C. Voigt, U. Schumann, I. Sölch, H. Schlager, S. Kaufmann, A. Petzold, D. Schäuble, and J.-F. Gayet (2013), Aircraft type influence on contrail properties, *Atmos. Chem. Phys.*, *13*, 11,965–11,984.

Kärcher, B. (2016), The importance of contrail ice formation for mitigating the climate impact of aviation, *J. Geophys. Res. Atmos.*, *121*, 3497–3505, doi:10.1002/2015JD024696.

Kärcher, B., U. Burkhardt, A. Bier, L. Bock, and I. J. Ford (2015), The microphysical pathway to contrail formation, *J. Geophys. Res. Atmos.*, *120*, 7893–7927, doi:10.1002/2015JD023491.

Kaufmann, S., C. Voigt, P. Jeßberger, T. Jurkat, H. Schlager, A. Schwarzenboeck, M. Klingebiel, and T. Thornberry (2014), In situ measurements of ice saturation in young contrails, *Geophys. Res. Lett.*, *41*, 702–709, doi:10.1002/2013GL058276.

Lamb, D., and J. Verlinde (2011), *Physics and Chemistry of Clouds*, Cambrigde Univ. Press, Cambridge, U. K.

Lewellen, D. C. (2012), Analytic solutions for evolving size distributions of spherical crystals or droplets undergoing diffusional growth in different regimes, *J. Atmos. Sci.*, *69*, 417–434.

Moore, R. H., et al. (2015), Influence of jet fuel composition on aircraft engine emissions: A synthesis of aerosol emissions data from the NASA APEX, AAFEX, and ACCESS missions, *Energy Fuels*, *29*, 2591–2600.

Moore, R. H., et al. (2017), Biofuel blending reduces particle emissions from aircraft engines at cruise conditions, *Nature*, *543*, 411–415, doi:10.1038/nature21420.

Naiman, A. D., S. K. Lele, and M. Z. Jacobson (2011), Large eddy simulations of contrail development: Sensitivity to initial and ambient conditions over first twenty minutes, *J. Geophys. Res.*, *116*, D21208, doi:10.1029/2011JD015806.

Noppel, F, and R. Singh (2007), Overview on contrail and cirrus cloud avoidance technology, *J. Aircr.*, *44*, 1721–1726.

Paoli, R., and K. Shariff (2016), Contrail modeling and simulation, *Annu. Rev. Fluid Mech.*, *48*, 393–427.

Schumann, U., P. Jeßberger, and C. Voigt (2013), Contrail ice particles in aircraft wakes and their climatic importance, *Geophys. Res. Lett.*, *40*, 2867–2872, doi:10.1002/grl.50539.

Sussmann, R. (1999), Vertical dispersion of an aircraft wake: Aerosol-lidar analysis of entrainment and detrainment in the vortex regime, *J. Geophys. Res.*, *104*(D2), 2117–2129.

Unterstrasser, S. (2014), Large-eddy simulation study of contrail microphysics and geometry during the vortex phase and consequences on contrail-to-cirrus transition, *J. Geophys. Res. Atmos.*, *119*, 7537–7555, doi:10.1002/2013JD021418.

Unterstrasser, S. (2016), Properties of young contrails—A parametrisation based on large-eddy simulations, *Atmos. Chem. Phys.*, *16*, 2059–2082.

Voigt, C., et al. (2010), In situ observations of young contrails—Overview and selected results from the CONCERT campaign, *Atmos. Chem. Phys.*, *10*, 9039–9056.

Wong, H.-W., and R. C. Miake-Lye (2010), Parametric studies of contrail ice particle formation in the jet regime using microphysical parcel modeling, *Atmos. Chem. Phys.*, *10*, 3261–3272.